



# OPEN Post-synthetic modification of Zr-based metal organic framework by schiff base zinc complex for catalytic applications in a click reaction

Mohammad-Aqa Rezaie, Amir Khojastehnezhad & Ali Shiri✉

A novel nanocatalyst, denoted as UiO-66/Sal-ZnCl<sub>2</sub>, has been synthesized and systematically characterized employing a range of analytical techniques, including Fourier-transform infrared spectroscopy (FT-IR), X-ray diffraction (XRD), transmission electron microscopy (TEM), scanning electron microscopy (SEM), energy-dispersive X-ray spectroscopy (EDX), thermogravimetric analysis (TGA), Brunauer–Emmett–Teller (BET) surface area analysis, and inductively coupled plasma (ICP) analysis. The comprehensive analyses collectively affirm the effective coordination of zinc chloride onto the functionalized UiO-66. Subsequently, the catalytic efficacy of UiO-66/Sal-ZnCl<sub>2</sub> was assessed in a one-pot, three-component click reaction involving terminal alkynes, alkyl halides, and sodium azide, conducted in an aqueous medium. The catalyst demonstrated remarkable catalytic activity, showcasing the capability to facilitate the reaction with high yields and exceptional regioselectivity. Noteworthy attributes of this nanocatalyst and the method include its elevated efficiency, recyclability, convenient product workup, and, significantly, the utilization of a sustainable solvent medium. The synthesis, characterization, and catalytic performance of this catalyst collectively contribute to its potential as an innovative and reusable nanocatalyst for diverse synthetic transformations.

**Keywords** Nanocatalyst, Metal organic framework, Click reaction, Post-synthetic modification, Triazole

In recent years, caused by concern about environmental issues, the advancement of supported heterogeneous catalysts has emerged as a significant challenge for scientists, attributed to their enhanced environmental compatibility, superior efficiency, and efficient recycling of catalysts<sup>1–4</sup>. Metal-organic frameworks (MOFs) as heterogeneous catalysts have attracted considerable attention within the scientific community due to their unique characteristics as porous crystalline coordination polymers. These attributes encompass a substantial surface area, remarkable porosity, facile structural adaptability, and the ability to be functionalized with diverse organic linkers, along with adjustable pore sizes. These features contribute to their remarkable performance as catalysts, particularly in catalytic organic transformations<sup>5–7</sup>. MOFs also have found applications as gas absorbers, storage devices and separators, water purifiers, sensors, magnets, photocatalysts, and in drug delivery systems<sup>8–15</sup>. Their porous structure, characterized by accessible and large cavities, facilitates the efficient transport of reactants into the internal regions of the framework. This enables effective interaction with the catalytically active sites, followed by the subsequent release of products from the pores into the reaction environment<sup>7,16</sup>. MOFs have been employed extensively in catalytic reactions, either by creating inherent acidic and basic sites on their surfaces or by serving as supports for other catalysts. They can be used directly, without any alterations to their structure, and the desired catalyst developed on the surface or in its pores<sup>16</sup>. Also, it is advisable to carry out a structural modification prior to the loading of efficient catalytic systems<sup>17</sup>. By means of post-synthesis modification of MOFs, it is possible to adjust their chemical and physical properties, as well as to introduce a diverse array of organic and inorganic functionalities<sup>18,19</sup>. Among various MOFs, Zirconium-based MOFs (Zr-MOFs) have garnered substantial attention in chemical research<sup>20</sup>. UiO-66, the first synthesized Zr-MOF, consists of a zirconium-oxo cluster and 1,4-benzenedicarboxylic acid. This MOF exhibits

Department of Chemistry, Faculty of Science, Ferdowsi University of Mashhad, Mashhad, Iran. ✉email: alishiri@um.ac.ir

unparalleled hydrothermal stability<sup>21</sup> and has been applied in water treatment<sup>22</sup>, remediation<sup>23</sup>, catalysis<sup>24</sup>, and various other fields<sup>25–28</sup>. Zr-MOFs have been employed in the synthesis of diverse organic compounds through multicomponent reactions<sup>29</sup>. Ionic liquid-supported Zr-MOF BAIL@UiO-66 was utilized in the preparation of pyrimidine and spirooxindole derivatives<sup>30,31</sup>. Pyrimidopyrimidines were prepared via TEDA-BAIL@UiO-66 catalyzed reaction<sup>32</sup>. Zr-MOF-FePC was reported for synthesis of  $\alpha$ -acyloxy amides<sup>33</sup>. Additionally, UiO-66 modified with ethylene diamine (ED), UiO-66-SO<sub>3</sub>H, and Zr-MOF have been employed for the synthesis of 2-aminotophenes<sup>34</sup>, dihydro-2-oxopyrroles<sup>35</sup>, imidazo[1,2-a]pyridines, 3,4-dihydroquinoxaline-2-amines, and trisubstituted pyridine derivatives<sup>36</sup>, respectively.

In the pursuit of novel catalytic systems for organic transformations<sup>37–41</sup>, this study presents the synthesis of a UiO-66 metal-organic framework post-modified with salicylaldehyde via Schiff base reaction, followed by coordination of Zinc chloride (UiO-66/Sal-ZnCl<sub>2</sub>). This method presents a robust catalyst for the efficient synthesis of 1,2,3-triazoles via a one-pot click coupling reaction involving terminal alkynes, aryl or alkyl halides, and sodium azide. Numerous methods have been developed for the synthesis of triazole derivatives, as recently reviewed<sup>42–44</sup>. Notable examples include the use of L-Proline-MCM-41-CuCl<sub>2</sub><sup>45</sup>, [(Cell-ThP-Cu(II))]<sup>46</sup>, Cell/SiO<sub>2</sub>-Sal-Pd(II)<sup>47</sup>, and CuLL<sub>1</sub>PPh<sub>3</sub> (L<sub>1</sub> = bis(pyrazolyl)methane)<sup>48</sup> as catalysts for triazole synthesis. Nevertheless, a majority of the aforementioned catalysts and methodologies encountered significant challenges, including the high cost of catalyst preparation, the use of hazardous solvents and reagents, and the difficulties associated with catalyst recovery techniques. Consequently, the imperative to develop a novel and efficient catalyst becomes paramount within the domain of organic synthesis. This imperative is particularly emphasized in the synthesis of triazole derivatives, where the inadequacies of existing catalysts and methods underscore the urgency and desirability of advancing catalytic approaches for enhanced efficacy and sustainability in the synthesis of such compounds.

## Experimental

All substrates, reagents, and solvents were procured from reputable suppliers, namely Merck and Aldrich. TEM Images were acquired using a Leo 912AB microscope at 120 kV and SEM images were acquired using a Leo 1450VP microscope. Thermogravimetric analyses were recorded with Mettler Toledo LF -Switzerland and FT-IR spectra with Nicolet Fourier spectrophotometer using KBr pellets. The energy dispersive X-ray analysis (XRD) was utilized to examine the crystalline structure of the catalyst. The <sup>1</sup>H- and <sup>13</sup>C-NMR spectra of the products were acquired in CDCl<sub>3</sub> solvent utilizing the Bruker DRX-300 AVANCE spectrometer operating at frequencies of 300 and 75 MHz, respectively.

### General procedure for the synthesis of UiO-66-NH<sub>2</sub>

According to the literature<sup>49</sup>, ZrCl<sub>4</sub> (11.652 g, 50 mmol) was dissolved in 250 ml DMF in a three-necked flask with vigorous stirring. Then 2-aminoterephthalic acid (9.058 g, 50 mmol) was added and stirred to give a yellow clear solution. Then concentrated HCl 37% (35 ml) was added to the flask with stirring and it was kept under reflux for 10 h. The suspension was then cooled to 30 °C and the light-yellow solid was filtered off. The precipitate was washed with DMF (2 × 10 ml) and deionized water (2 × 10 ml) and dried at 70 °C for 6 h to prepare UiO-66-NH<sub>2</sub>.

### General procedure for the synthesis of UiO-66-Sal

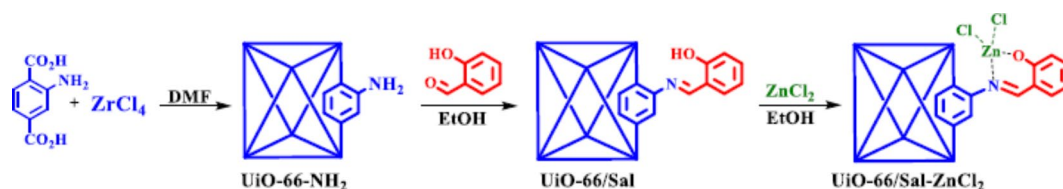
UiO-66-NH<sub>2</sub> (0.15 g) was dispersed in absolute ethanol (100 ml) by sonication and then stirred with salicylaldehyde (1250  $\mu$ L, 12 mmol) at 75 °C for 12 h. After this time, the mixture was cooled to 30 °C, then the solid was filtered, washed with water and ethanol (3 × 15 ml), and dried overnight at 75 °C (UiO-66/Sal)<sup>42</sup>.

### General procedure for the synthesis of UiO-66/Sal-ZnCl<sub>2</sub>

The prepared UiO-66/Sal salt (0.15 g) and zinc chloride (0.82 g, 0.6 mmol) were dispersed in absolute ethanol (20 ml), and the suspension was then stirred for 24 h at 50 °C. The prepared solid catalyst was filtered off, washed with absolute ethanol (3 × 20 ml), and dried at 70 °C for 12 h (UiO-66/Sal-ZnCl<sub>2</sub>).

### General procedure for the synthesis of 1,2,3-Triazoles

Phenylacetylene (1 mmol), sodium azide (1 mmol), halide (1 mmol), and UiO-66/Sal-ZnCl<sub>2</sub> (20 mg) were mixed in water (2 mL) and stirred at 50 °C for the appropriate time. The progress of the reaction was monitored by thin-layer chromatography (TLC). After completion of the reaction, the reaction mixture was cooled to 30 °C and the catalyst was filtered off. The reaction mixture underwent extraction using a combination of ethyl acetate and water, followed by the subsequent evaporation of the organic layer. Subsequently, the product was subjected to a drying process at a temperature of 50 °C for 4 h.



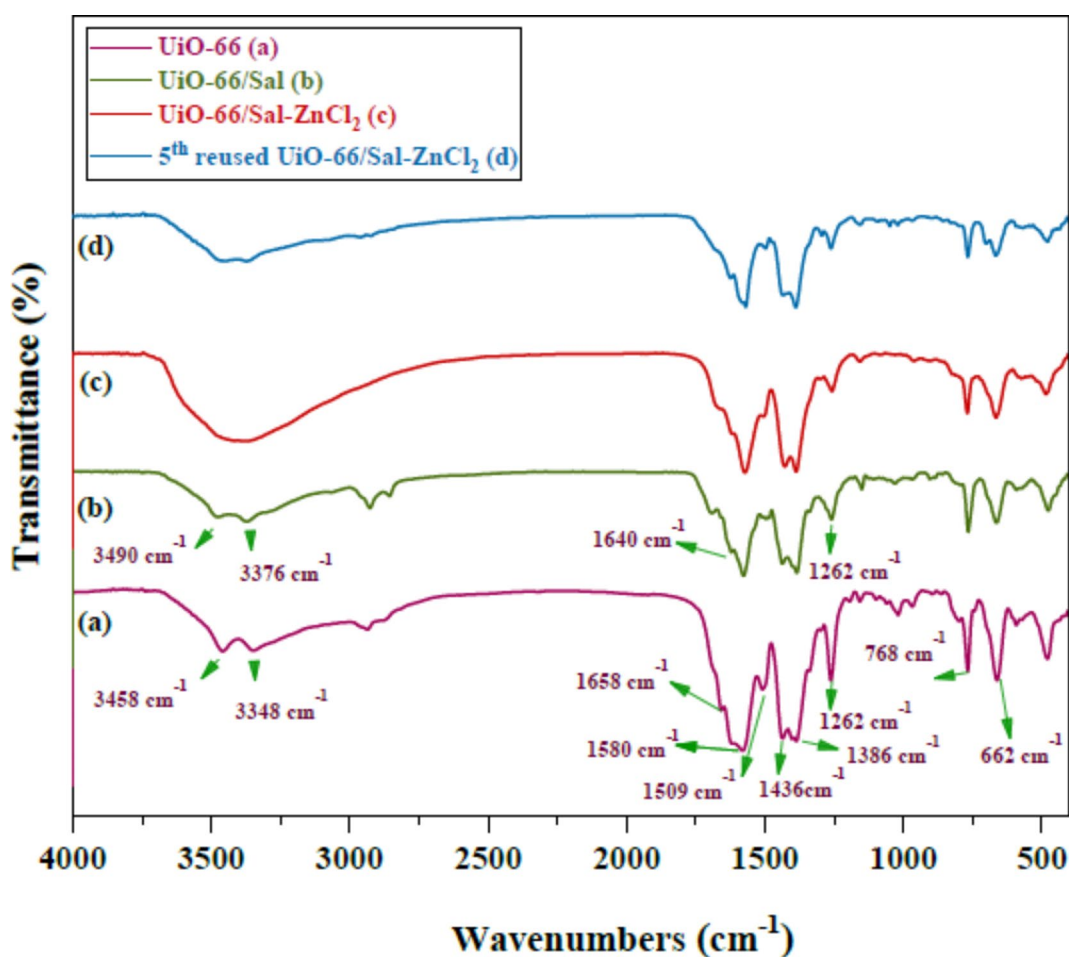
**Fig. 1.** The synthetic pathway for the production of UiO-66/Sal-ZnCl<sub>2</sub>.

## Results and discussion

The synthesis of the heterogeneous UiO-66/Sal-ZnCl<sub>2</sub> nanocatalyst was successfully accomplished through a three-step synthetic procedure. Initially, UiO-66-NH<sub>2</sub> was synthesized by combining ZrCl<sub>4</sub> and 2-aminoterephthalic acid. Subsequently, the -NH<sub>2</sub> groups were chemically reacted with salicylaldehyde in a post-modification step, resulting in the formation of UiO-66/Sal. Finally, the coordination of ZnCl<sub>2</sub> salt with UiO-66/Sal led to the formation of UiO-66/Sal-ZnCl<sub>2</sub>, as illustrated in Fig. 1. The chemical structure of prepared catalyst (UiO-66/Sal-ZnCl<sub>2</sub>) was confirmed using various techniques, including ICP, FT-IR, TGA, BET, TEM, SEM, EDX, and XRD, as detailed in this section.

The quantification of zinc ions on the UiO-66/Sal-ZnCl<sub>2</sub> nanocatalyst was conducted through ICP-OES analysis. The zinc concentration was determined to be 0.501 wt% of the catalyst.

The chemical structure and functional groups of UiO-66-NH<sub>2</sub>, UiO-66/Sal, and UiO-66/Sal-ZnCl<sub>2</sub> were examined via FT-IR analysis, as depicted in Fig. 2. For UiO-66-NH<sub>2</sub> (Fig. 2a), peaks at 3458 and 3348 cm<sup>-1</sup> were assigned to asymmetric and symmetric vibrations, while the 1658 cm<sup>-1</sup> peak indicated the bending vibration of NH<sub>2</sub> groups. The symmetric and asymmetric stretching vibrations of carboxyl groups associated with Zr<sup>4+</sup> were observed at 1580 and 1386 cm<sup>-1</sup>, respectively. A peak at 1509 cm<sup>-1</sup> corresponded to the stretching vibration of C=C units in benzene rings, while the shear vibration of N-H groups appeared at 1436 cm<sup>-1</sup>. Additionally, a unique C-N stretching absorption of aromatic amines was evident at 1262 cm<sup>-1</sup>. Peaks at 768 and 662 cm<sup>-1</sup> were attributed to the stretching vibration of μ<sub>3</sub>-O in Zr-(OC)<sup>50,51</sup>. After salicylaldehyde modification of UiO-66-NH<sub>2</sub>, the characteristic amine group peaks disappeared (Fig. 2b), the absorbance peaks observed at 3490 and 3376 cm<sup>-1</sup> belong to the stretching vibrations of -OH and -NH bonds, respectively. Also, an imine bond (C=N) stretching vibrations of the Schiff base was appeared at 1640 cm<sup>-1</sup><sup>152,53</sup>, indicating successful post-modification. Notably, the FT-IR spectrum of UiO-66/Sal-ZnCl<sub>2</sub> (Fig. 2c) did not exhibit characteristic peaks of ZnCl<sub>2</sub>, possibly due to the weak bands associated with immobilized zinc ions on the nanocatalyst's surface<sup>54</sup>. On the other hand, the decrease in the vibrational frequencies in the range of 3490–3376 cm<sup>-1</sup> are confirmed the successfully interaction between nitrogen (imine group) and hydroxyl groups with Zn ions. Figure 2d presents the FT-IR spectrum of the catalyst after five cycles of reuse, which appears identical to that of the fresh catalyst



**Fig. 2.** FTIR spectrum of UiO-66-NH<sub>2</sub> (a), UiO-66/Sal (b), UiO-66/Sal-ZnCl<sub>2</sub> (c), 5th reused UiO-66/Sal-ZnCl<sub>2</sub> (d).

(Fig. 2c). This result indicates that the catalyst structure remains stable and that the organic reaction condition did not affect its integrity.

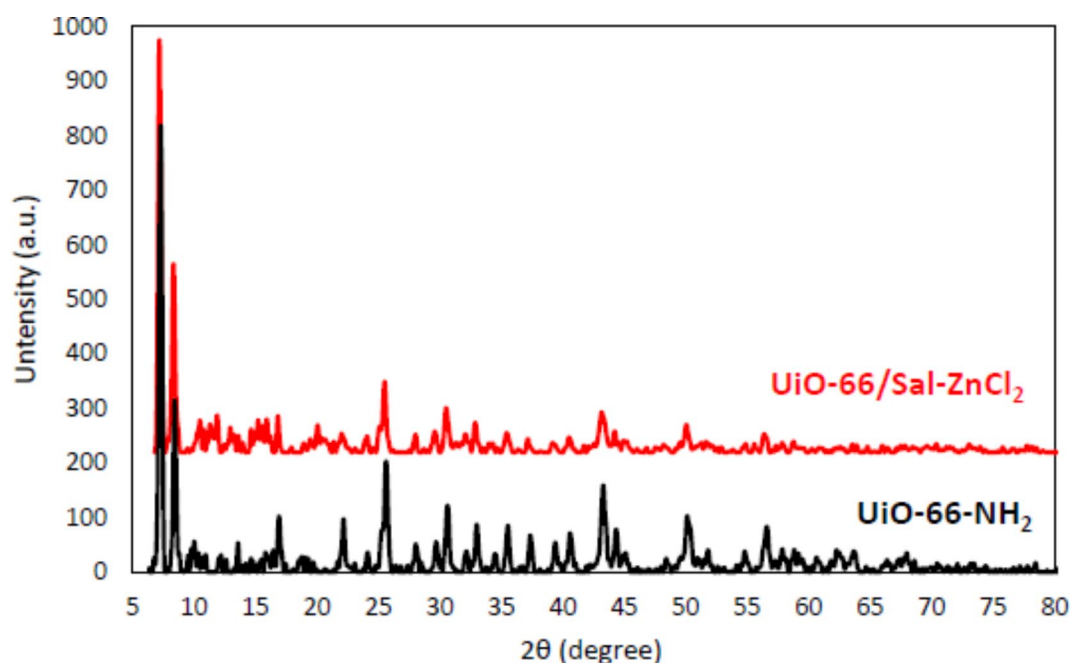
The crystalline structure of UiO-66-NH<sub>2</sub> and UiO-66/Sal-ZnCl<sub>2</sub> was investigated using XRD analysis within the 2θ range of 6–80° (Fig. 3). The XRD pattern of UiO-66-NH<sub>2</sub> (Fig. 3a) displayed characteristic diffraction peaks at 2θ values of 7.5°, 8.7°, 14.6°, 17.5°, 22.3°, 25.6°, 30.5°, 31.2°, 35.9°, 37.8°, 40.2°, 43.5°, 50.6°, and 56.9°, corresponding to the crystal lattice with Fm3m symmetry of zirconium benzene carboxylate units<sup>55</sup>. These diffraction peaks were also observed in the XRD pattern of UiO-66/Sal-ZnCl<sub>2</sub> (Fig. 3b), indicating that the catalyst's crystalline structure remained unchanged after modification and coordination of zinc units on the surface. The characteristic peaks of ZnCl<sub>2</sub> should be at 2θ of 16.2°, 17.2°, 26.0°, 29.9°, 35.5°, 38.9°, 49.3°, 49.8°, 51.9°, 52.9°, and 56.8° (JCPDS card no. 96-810-3830)<sup>56</sup> (Trivedi et al., 2017), however the intensity of these expected peaks was quite low, likely due to the results from the ICP analysis and the relatively low metal loading.

As depicted in Fig. 4, the elemental composition of UiO-66-NH<sub>2</sub> and UiO-66/Sal-ZnCl<sub>2</sub> was determined through EDX analysis. In the EDX spectrum of UiO-66-NH<sub>2</sub> (Fig. 4a), signals corresponding to Zirconium (Zr), Oxygen (O), and Nitrogen (N) were observed, representing the primary elements of the intended MOF structure<sup>57</sup>. In the case of UiO-66/Sal-ZnCl<sub>2</sub>, EDX analysis (Fig. 4b), these expected elements (Zr, O, and N) were again observed, alongside the presence of elemental zinc and chlorine<sup>57</sup>.

Following the elemental composition analysis, the distribution of these elements on the catalyst's surface was examined. Figure 5 presents the X-ray elemental mapping of UiO-66/Sal-ZnCl<sub>2</sub>, demonstrating the even dispersion of elements within the catalyst framework. Zirconium (Zr), being the fundamental building block with a considerably higher density compared to other elements, exhibited a uniform distribution. This observation further underscores the crucial role of uniform zinc (Zn) distribution within the catalyst matrix, which contributes significantly to its exceptional catalytic performance. These observations are in agreement with ICP and EDX analyses and confirm the successful coordination of Zn complexes onto the surface of modified MOF.

In order to ascertain the loading capacity of the organic linker and examine the thermal stability of UiO-66-NH<sub>2</sub> and UiO-66/Sal-ZnCl<sub>2</sub>, thermal gravimetric analysis (TGA) was conducted across a temperature range spanning from 25 to 700 °C (Fig. 6). Three weight losses were observed in the thermogravimetric analysis (TGA) curve of UiO-66-NH<sub>2</sub>, as depicted in Figure (Fig. 6a). The initial weight reduction step, occurring up to 150 °C, involved the removal of trapped water, solvent, and CO<sub>2</sub> molecules. During the second phase of weight loss, occurring at temperatures exceeding 180 °C, the organic linker initiates decomposition. The third stage of weight loss, occurring between 350 °C and 500 °C, can be attributed to the complete disassembly of the framework. In the case of UiO-66/Sal-ZnCl<sub>2</sub>, a greater weight loss was observed during this stage compared to UiO-66-NH<sub>2</sub>, primarily due to the presence of a surface-bound organic linker (Fig. 6b)<sup>58</sup>. From these results, the amount of organic linker was estimated to be about 6% by weight. These results are in accordance with other analyses and approve the successful synthesis and post-synthetic modification of UiO-66.

The porous structures of UiO-66-NH<sub>2</sub> and UiO-66/Sal-ZnCl<sub>2</sub> were characterized using N<sub>2</sub> adsorption-desorption analysis (Fig. 7). According to Brunauer-Emmett-Teller (BET) analysis, the surface areas of UiO-66-NH<sub>2</sub> and UiO-66/Sal-ZnCl<sub>2</sub> were measured to be 909.59 and 550.11 m<sup>2</sup>g<sup>-1</sup>, respectively (Fig. 7a and b). The observed reduction in surface area for UiO-66/Sal-ZnCl<sub>2</sub> compared to UiO-66-NH<sub>2</sub> suggests that the post-



**Fig. 3.** XRD patterns of UiO-66-NH<sub>2</sub> (black PXRD pattern), and UiO-66/Sal-ZnCl<sub>2</sub> (red thin-layer PXRD pattern).

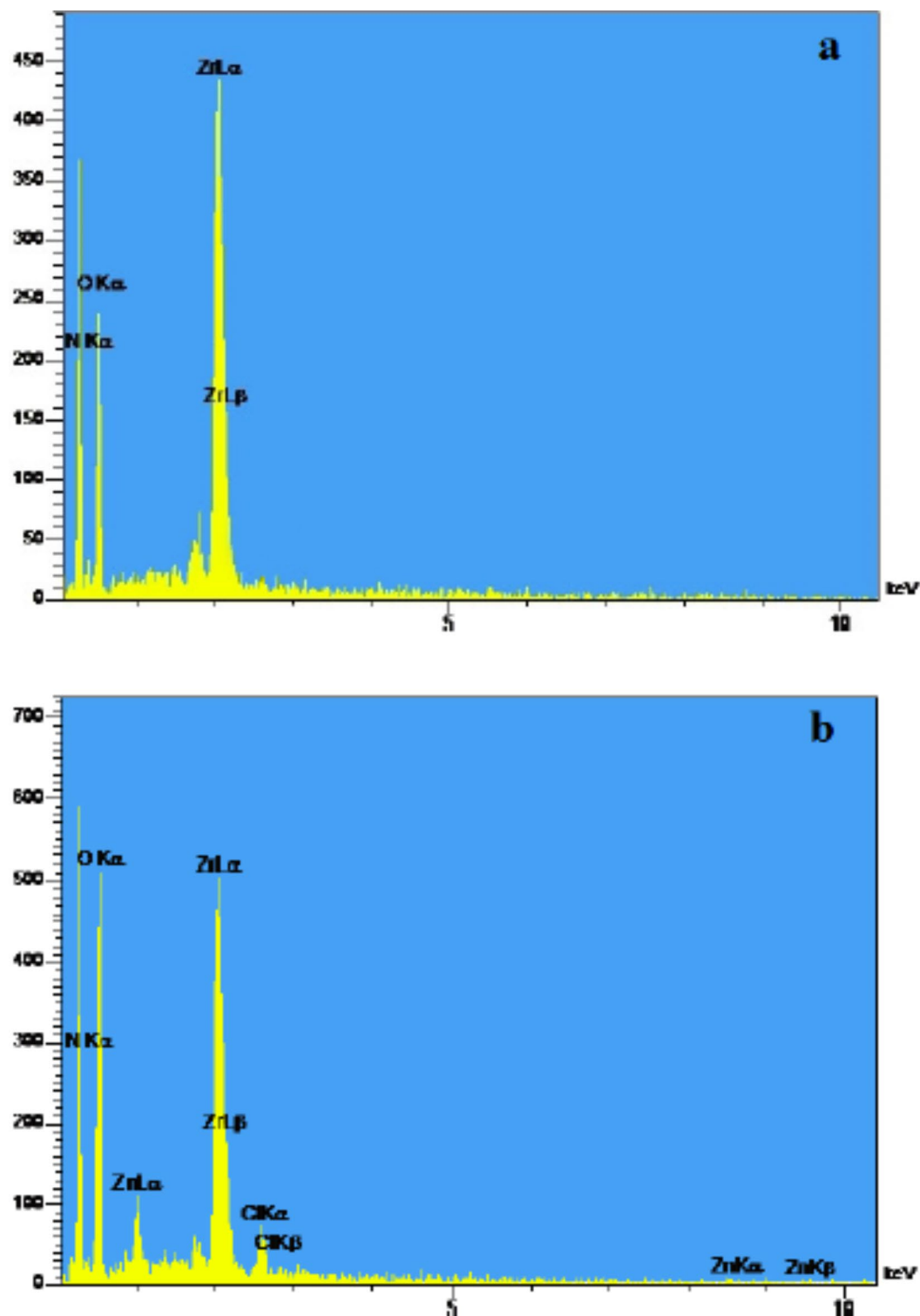
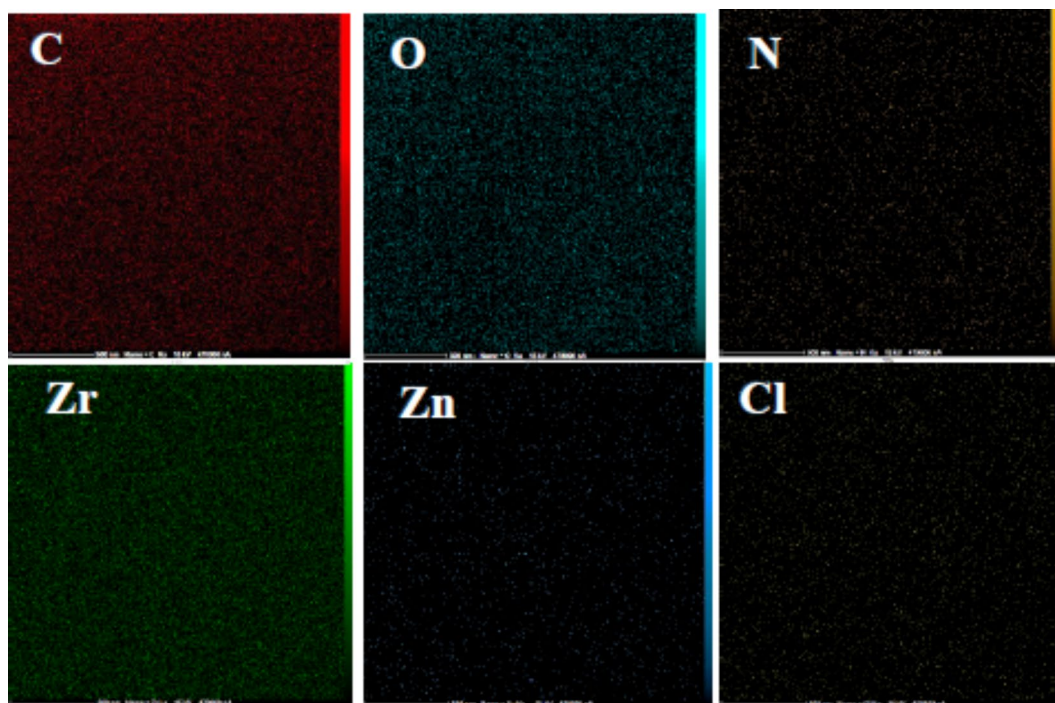


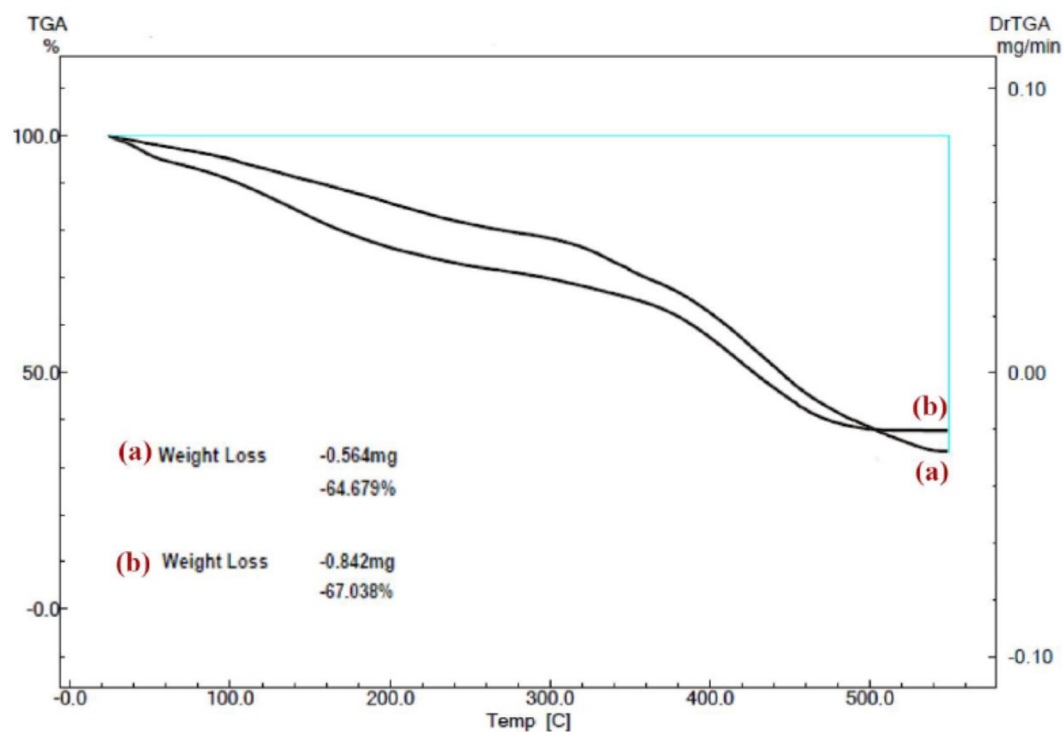
Fig. 4. EDX analysis of (a) UiO-66-NH<sub>2</sub>, and (b) UiO-66/Sal-ZnCl<sub>2</sub>.

modification and coordination steps involving ZnCl<sub>2</sub> primarily occurred on the support surface. The adsorption-desorption isotherm of UiO-66-NH<sub>2</sub> displayed a type I isotherm, indicative of a microporous structure (Fig. 7a). The Barrett-Joyner-Halenda (BJH) diagram for UiO-66-NH<sub>2</sub> revealed the presence of a single type of micropores with a pore diameter of 1.21 nm (Fig. 7c). Similarly, the BJH plot for UiO-66/Sal-ZnCl<sub>2</sub> also indicated reduced-intensity micropores, consistent with changes in surface area and pore filling resulting from the coordination of the zinc salt (Fig. 7d)<sup>58</sup>.

Electron microscopy analyses, including TEM and SEM, were conducted to assess the morphology and size distribution of the synthesized samples (Fig. 8). The TEM images of UiO-66-NH<sub>2</sub> and UiO-66/Sal-ZnCl<sub>2</sub>

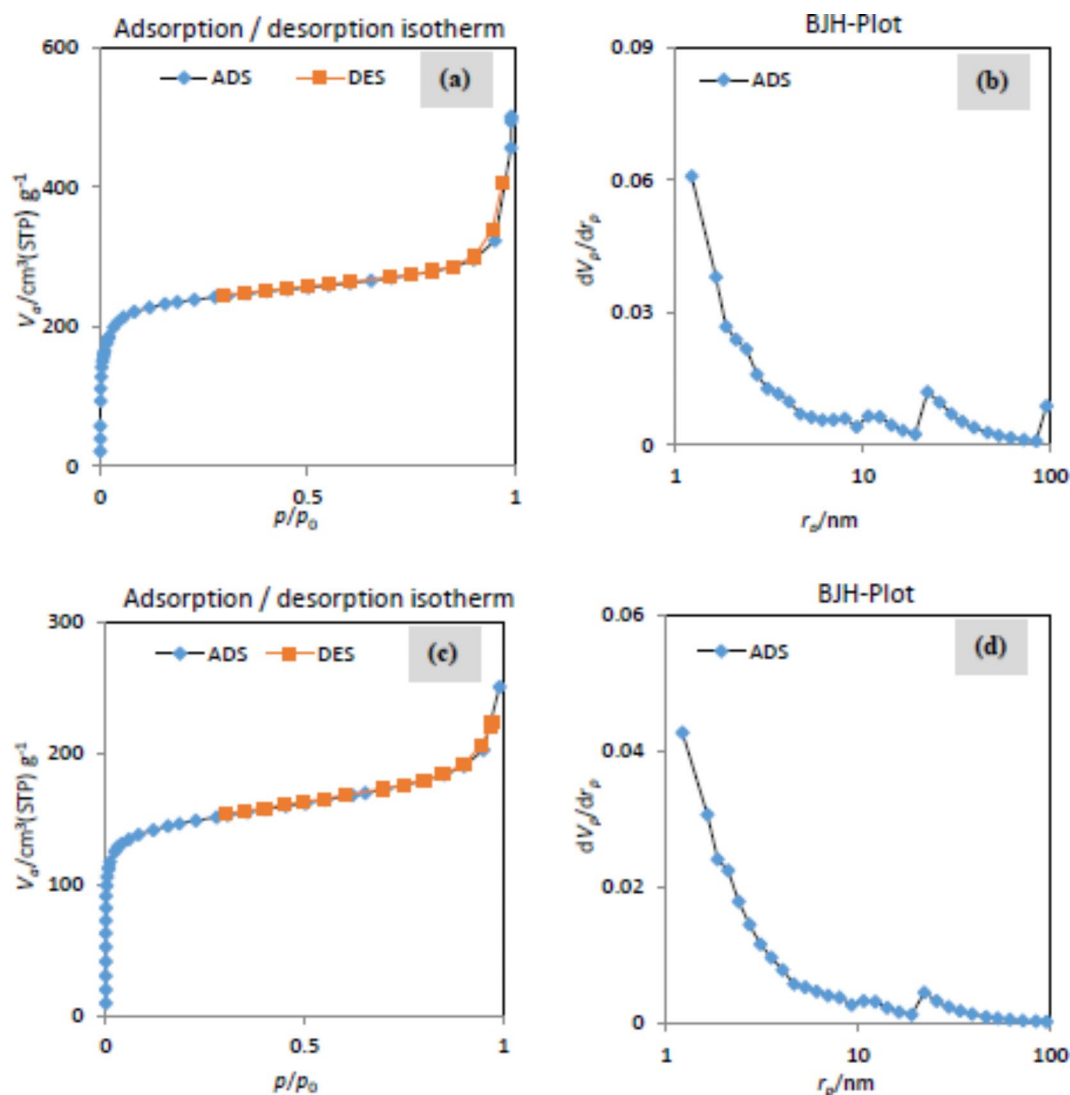


**Fig. 5.** Elemental mapping of UiO-66/Sal-ZnCl<sub>2</sub> (the atomic distribution: Zr, O, C, N, Cl and Zn).



**Fig. 6.** TGA curve of UiO-66-NH<sub>2</sub> (a), and UiO-66/Sal-ZnCl<sub>2</sub> (b).

revealed aggregated octahedral particles with sizes ranging from 30 to 100 nm (Fig. 8a and b). Notably, the TEM image of UiO-66/Sal-ZnCl<sub>2</sub> exhibited a similar morphology to the unmodified MOF, indicating that the post-synthetic modification with salicylaldehyde and subsequent zinc coordination did not significantly alter the MOF's structural morphology and sizes (Fig. 8b). Furthermore, SEM analysis has been conducted for both UiO-66-NH<sub>2</sub> and UiO-66/Sal-ZnCl<sub>2</sub> (Fig. 8d and e) and the images exhibited aggregated octahedral particles for

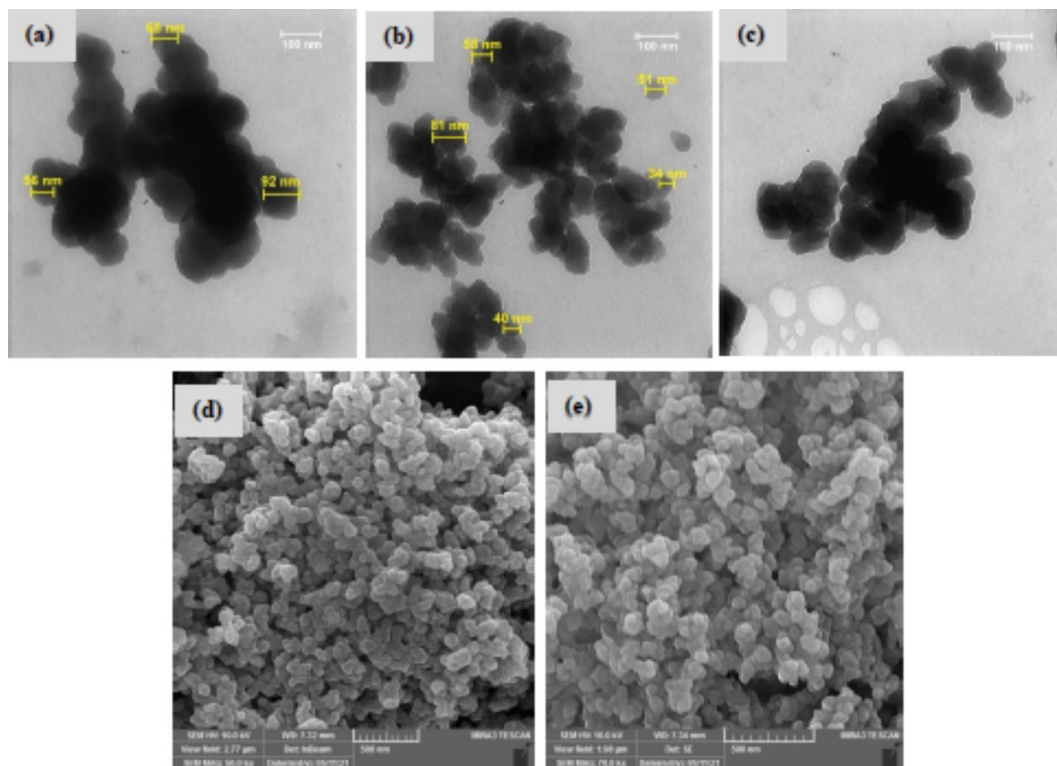


**Fig. 7.** The BET of UiO-66-NH<sub>2</sub> (a), and UiO-66/Sal-ZnCl<sub>2</sub> (b), BJH of UiO-66-NH<sub>2</sub> (c), and UiO-66/Sal-ZnCl<sub>2</sub> (d).

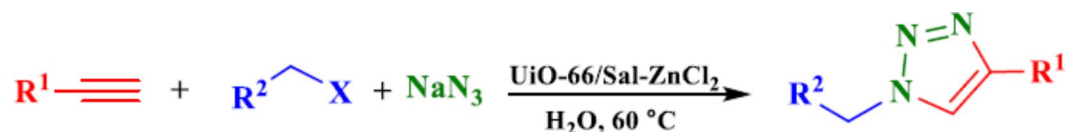
two materials before and after post-synthetic modification and zinc coordination, confirming the preservation of the MOF's morphology throughout the modification and coordination processes.

Following the successful synthesis and characterization of UiO-66/Sal-ZnCl<sub>2</sub>, its catalytic activity was evaluated in a one-pot multicomponent reaction involving benzyl halides/alkyl halides, phenylacetylene/propargyl alcohol, and sodium azide for the synthesis of 1,2,3-triazole, as depicted in Fig. 9.

In this specific context, a comprehensive analysis was conducted to investigate the influence of various parameters, including reaction time, solvent, temperature, and catalyst quantity. Initially, the selection of phenylacetylene, benzyl bromide, and NaN<sub>3</sub> was made as model substrates to optimize the reaction conditions, as presented in Table 1. It was observed that the model reaction failed to proceed in absence of catalyst, even after 3 h in water at 60 °C, thereby confirming the essential role of the catalyst in facilitating the reaction (Table 1, entry 1). In model reactions catalyzed by UiO-66-NH<sub>2</sub> and ZnCl<sub>2</sub>, the product yields were only 30% and 15%, respectively (Table 1, entries 2 and 3). However, upon the addition of 5 mol% UiO-66/Sal-ZnCl<sub>2</sub> as a catalyst in the model reaction, the yield of the isolated product reached 98% (Table 1, entry 4). Various polar and nonpolar solvents were examined while using UiO-66/Sal-ZnCl<sub>2</sub> as the catalyst (Table 1, entries 5–9). Ultimately, considering the green nature of water and the achieved yield, water was chosen as the reaction solvent for further investigation. Model reactions were monitored at different time intervals, such as 2, 1, and 0.5 h. The results indicated that the reaction was completed after 2 h (Table 1, entries 10–12). Different quantities of catalysts were also tested in the model reaction. It was observed that the product yield decreased from 5 to 3.1 mol% with decreasing catalyst loading (Table 1, entries 13 and 14). Additionally, the reaction temperature was evaluated, revealing a decrease in yield with decreasing temperature. Consequently, the optimal reaction conditions were determined as follows: phenylacetylene (1.0 mmol), benzyl bromide (1.0 mmol), sodium azide (1.0 mmol), and a catalyst (5 mol%) in an aqueous medium at a temperature of 60 °C for 2 h.



**Fig. 8.** The TEM images of UiO-66-NH<sub>2</sub> (a), and UiO-66/Sal-ZnCl<sub>2</sub> (b), 5th reused UiO-66/Sal-ZnCl<sub>2</sub> (c), SEM images of UiO-66-NH<sub>2</sub> (d), UiO-66/Sal-ZnCl<sub>2</sub> (e).



**R<sup>1</sup> = Ph, CH<sub>2</sub>OH**

**R<sup>2</sup> = Aryl, Alkyl, X = Cl, Br**

**Fig. 9.** The UiO-66/Sal-ZnCl<sub>2</sub> catalyzed click reaction.

The versatility of UiO-66/Sal-ZnCl<sub>2</sub> was further explored with different substrates under the optimized reaction conditions. Substituted phenylacetylene and propargyl alcohol were successfully converted to terminal alkynes and benzyl /alkyl halides (Table 2). Employing various terminal alkynes, corresponding triazoles were obtained with exceptional performance under these optimal conditions. Additionally, a range of aryl and alkyl halides exhibited favorable reactivity in the presence of UiO-66/Sal-ZnCl<sub>2</sub>, as demonstrated in Table 2.

The potential for reusing the UiO-66/Sal-ZnCl<sub>2</sub> catalyst was also evaluated. In this investigation, the model reaction was performed using a fresh catalyst under the optimized condition. Upon confirming the completion of the reaction through thin-layer chromatography (TLC), the catalyst was subjected to filtration, followed by multiple washes with water and ethyl acetate. Subsequently, the recovered catalyst was dried in an oven at 70 °C. Remarkably, this regenerated catalyst demonstrated activity for five consecutive cycles in model reactions with new substrates. The efficiency of the catalyst slightly decreased from 99% in the first cycle to 86% in the last one, as illustrated in Fig. 10.

A plausible mechanism<sup>59–61</sup> for a model click reaction catalyzed by UiO-66/Sal-ZnCl<sub>2</sub> is shown in Fig. 11. In the first step, coordination between the catalyst and the terminal alkyne transforms the activated acetylene (I) into a more potent dienophile. In the next step, the intermediate alkyl azide formed by the reaction of alkyl halide and sodium azide interacts with complex (I) to form complex (II). Complex (II) gives complex (III) *via* a 1,3-dipolar cycloaddition reaction. The final step converts the complex (III) to the desired triazole (IV) and regenerates the catalyst.



Entry	Catalyst	Catalyst amount	Solvent	Temp. (°C)	Time (h)	Yield (%)
1	–	–	Water	60	3	0
2	UiO-66-NH <sub>2</sub>	0.1 g	Water	60	3	30
3	ZnCl <sub>2</sub>	0.1 g	Water	60	3	15
4	UiO-66/Sal-ZnCl <sub>2</sub>	5 mol%	Water	60	3	98
5	UiO-66/Sal-ZnCl <sub>2</sub>	5 mol%	EtOH	60	3	95
6	UiO-66/Sal-ZnCl <sub>2</sub>	5 mol%	DMF	60	3	96
7	UiO-66/Sal-ZnCl <sub>2</sub>	5 mol%	Toluene	60	3	65
8	UiO-66/Sal-ZnCl <sub>2</sub>	5 mol%	Hexane	60	3	50
9	UiO-66/Sal-ZnCl <sub>2</sub>	5 mol%	CH <sub>3</sub> CN	60	3	85
10	UiO-66/Sal-ZnCl <sub>2</sub>	5 mol%	Water	60	2	98
11	UiO-66/Sal-ZnCl <sub>2</sub>	5 mol%	Water	60	1	70
12	UiO-66/Sal-ZnCl <sub>2</sub>	5 mol%	Water	60	0.5	50
13	UiO-66/Sal-ZnCl <sub>2</sub>	3 mol%	Water	60	2	80
14	UiO-66/Sal-ZnCl <sub>2</sub>	1 mol%	Water	60	2	70
15	UiO-66/Sal-ZnCl <sub>2</sub>	5 mol%	Water	50	2	85
16	UiO-66/Sal-ZnCl <sub>2</sub>	5 mol%	water	40	2	65

**Table 1.** The optimized reaction conditions for the synthesis of triazole via the model reaction. Reaction conditions: phenylacetylene (1.0 mmol), benzyl bromide (1.0 mmol), sodium azide (1.0 mmol), catalyst (x mol%), and solvent (2 ml).

### Hot filtration test

The hot filtration test was conducted to evaluate the possible leaching of zinc ions during the reaction (Fig. 12). Precisely, at the midway of the reaction (60 min), the nanocatalyst was separated from the reaction mixture by filtration. In this step, only 53% conversion was achieved. Subsequently, the reaction mixture was allowed to continue without a catalyst for another 60 min under similar conditions. The reaction progress before and after the separation was checked by TLC. Assessment of the rate of the desired product preparation demonstrates that no remarkable increase in conversion was observed even after an expanded time.

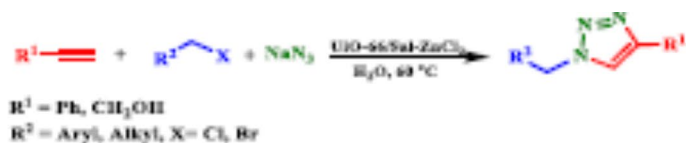
Also, to elucidate the stability of the catalyst, after five cycles in the model reaction, any structural changes of the catalyst were studied by FT-IR, TEM and ICP-OES techniques. It is evident from the FT-IR spectrum of the 5th reused catalyst that no significant changes in the frequencies, intensities, and shapes of absorption bands were observed (Fig. 1d). Moreover, the TEM image of the 5th reused catalyst confirmed the aggregated octahedral particles measuring less than 50 nm in size which was approximately similar to the TEM image of the fresh catalyst, and there were not any significant differences in size and morphology (Fig. 8c). Regarding the ICP-OES analysis, the exact quantity of zinc was 0.501 wt% in the fresh catalyst, which was decreased to 0.492 wt% and demonstrated a negligible leaching of Zn ions in the reaction medium after 5th iteration (less than 0.01 wt%). These results confirmed the admirable structural and mechanical stabilities of the reused catalyst after five reuse cycles.

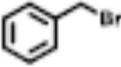
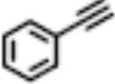
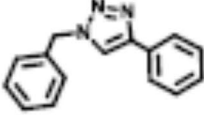
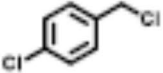
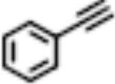
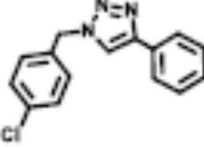
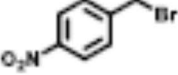
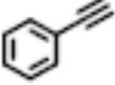
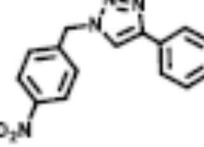
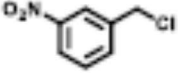
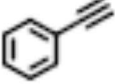
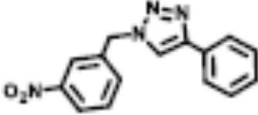

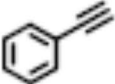
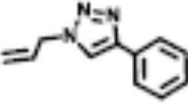

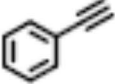
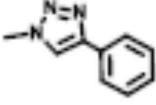

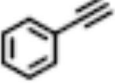
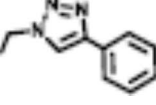
By knowing the effectiveness of the prepared nanocatalyst, a comparison investigated between its catalytic performance and that of zinc-based catalyst systems documented in the existing literature in the reaction of benzyl bromide, sodium azide, and phenylacetylene under various catalytic conditions (Table 3, entries 1–7).

Nearly all the catalysts mentioned below exhibit notable yields of the desired products. However, the limitations including the long reaction time (Table 3, entries 1 & 2), the high reaction temperature (Table 3, entries 1, 3 & 5), and applying hazardous solvent and reaction conditions (Table 3, entries 2 & 4) represent the drawbacks of some of these methods. As is evident, our studied system (Table 3, entry 6) has advantages such as an excellent yield in a shorter reaction time, simple separation, easy preparation of the catalyst, and milder reaction conditions. Although some reported catalysts have demonstrated the ability to catalyze the azide-alkyne reaction in shorter or comparable reaction times, our catalyst has achieved a higher yield in comparison to these reports (Table 3, entries 3–5).

### Conclusion

In conclusion, the UiO-66/Sal-ZnCl<sub>2</sub> catalyst was successfully synthesized using a post-modification approach. A comprehensive characterization of the catalyst was carried out utilizing various techniques, including TEM, SEM, FTIR, ICP, TGA, Mapping, XRD, and BET. The results confirmed the effective incorporation of Zn units into the UiO-66-NH<sub>2</sub> post-modified salicylaldehyde nanoreactor. Importantly, the morphology of the catalyst remained unaltered throughout the modification and coordination processes. The UiO-66/Sal-ZnCl<sub>2</sub> catalyst exhibited remarkable catalytic activity in the click reaction involving benzyl halides/alkyl halides, phenylacetylene/propargyl alcohol, and sodium azide, leading to the synthesis of 1,2,3-triazole. Furthermore, this catalyst displayed reusability, retaining its activity for five consecutive cycles. These findings underscore the potential of UiO-66/Sal-ZnCl<sub>2</sub> as an efficient and recyclable nanocatalyst for click reactions and related applications.



Entry	Benzyl/Alkyl halide	Alkyne	Product	Time (h)-Yield (%) <sup>a</sup>
1				2-98
2				2.5-96
3				2.5-94
4				3-92
5				3-93
6				3-92
7				3.5-93

**Table 2.** Synthesis of 1,4-disubstituted 1,2,3-triazoles using UiO-66/Sal-ZnCl<sub>2</sub>. Reaction conditions: alkyne (1 mmol), sodium azide (1 mmol), benzyl /alkyl halide (1 mmol), UiO-66/Sal-ZnCl<sub>2</sub> (5 mol%), water (2 mL), 60 °C. <sup>a</sup>Isolated yields.

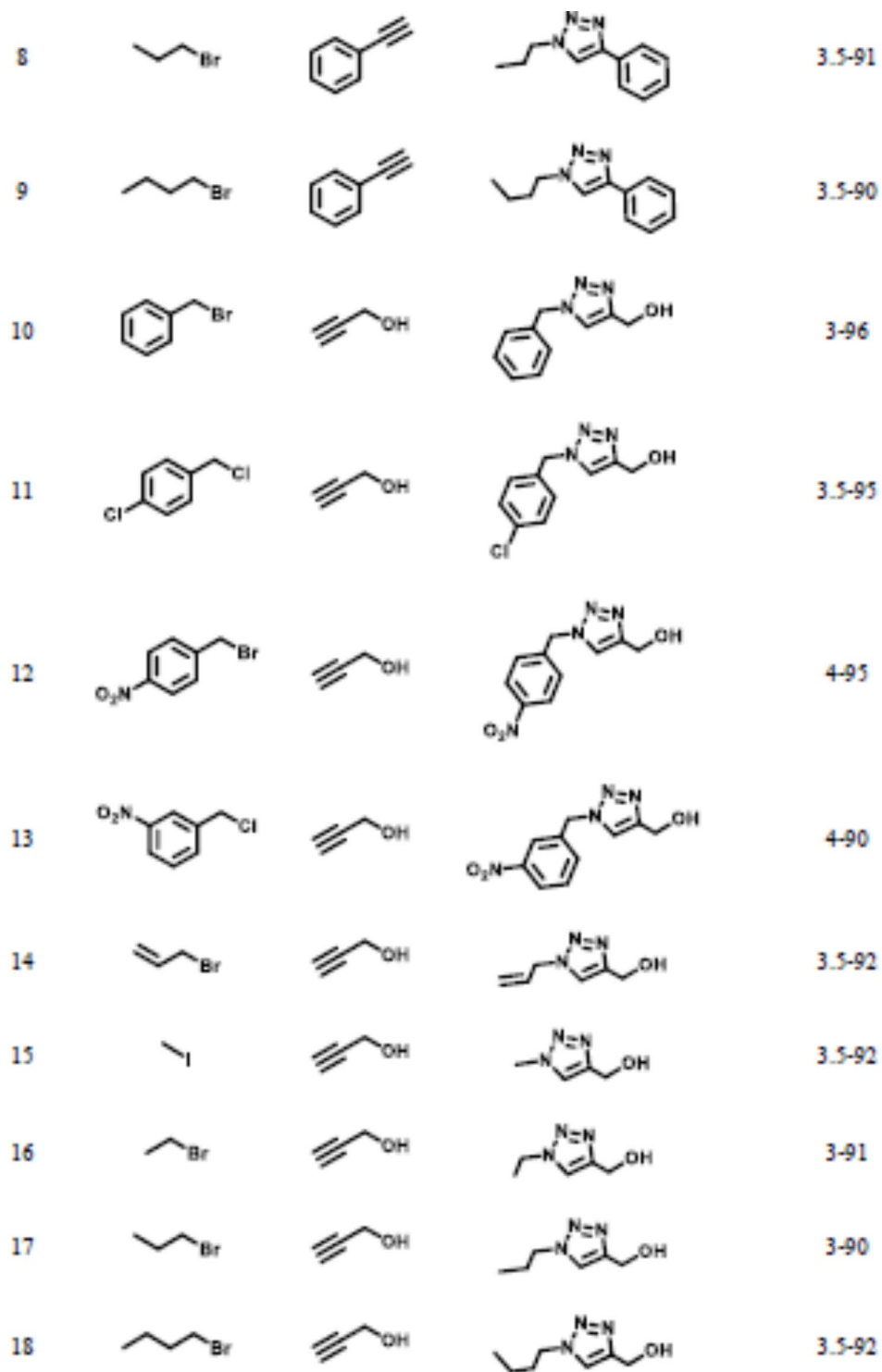


Figure 2. (continued)

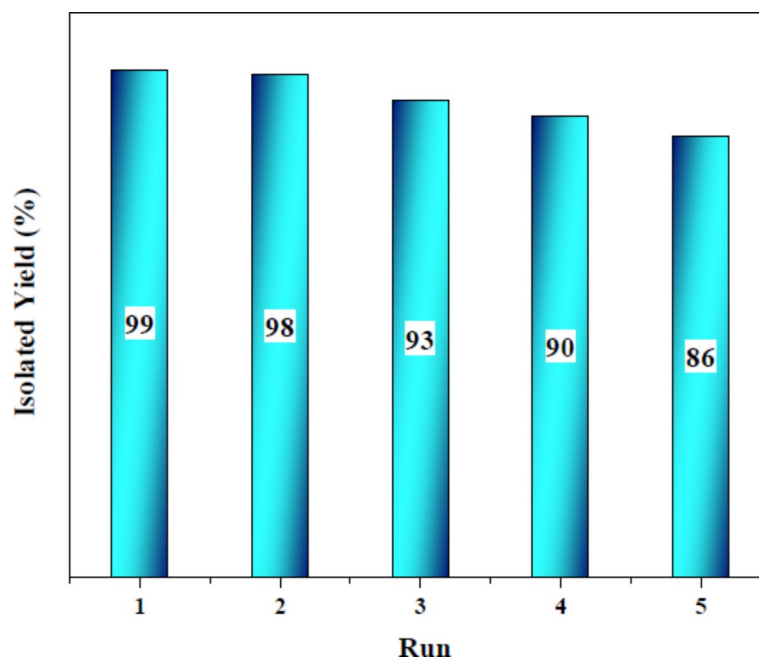


Fig. 10. The study of the catalyst recyclability.

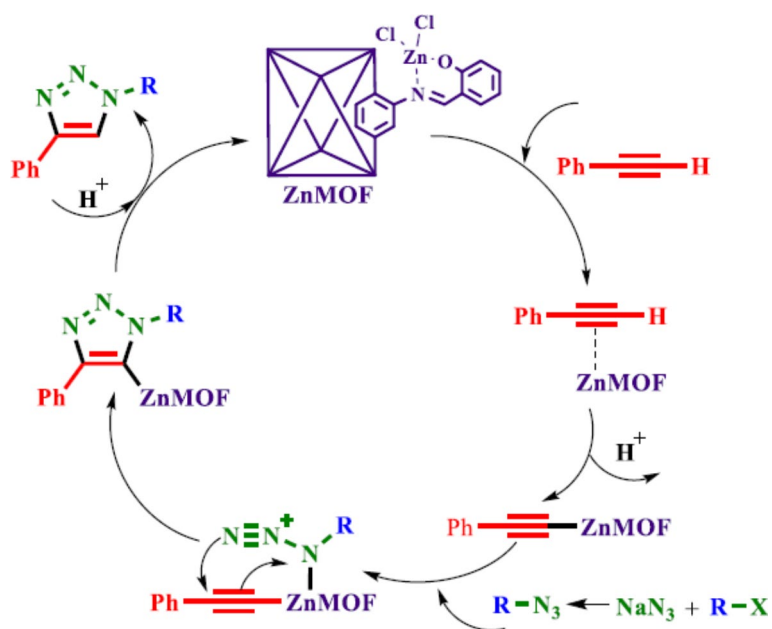
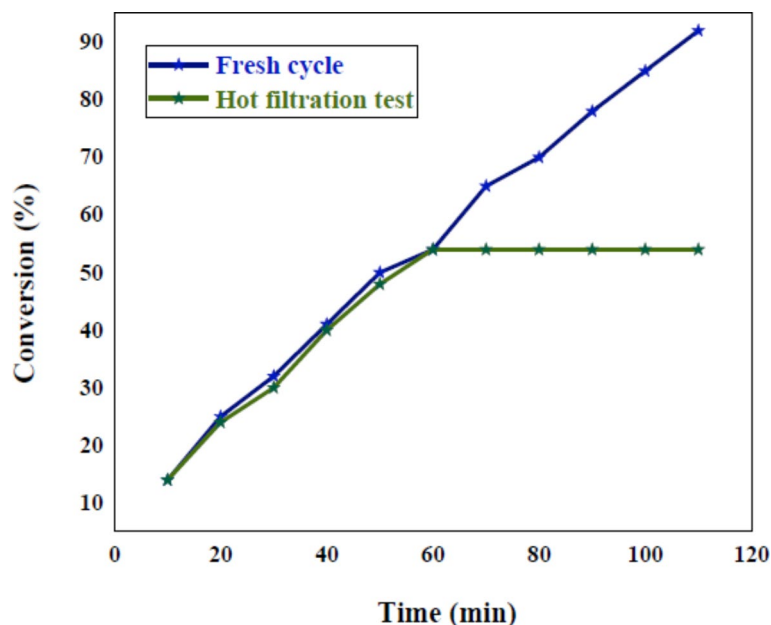


Fig. 11. Plausible mechanistic route for the UiO-66/Sal-ZnCl<sub>2</sub> mediated synthesis of triazoles.



**Fig. 12.** Time-dependent correlation of the product yield in hot filtration test.

Entry	Catalyst	Solvent	Temp.(°C)	Time (h)	Yield (%)	Refs.
1	Zn(OAc) <sub>2</sub> /ascorbic acid	Water	75	6.0	87	<sup>59</sup>
2	Zn/C	DMF	50	15	90	<sup>62</sup>
3	GO-Salen-Zn	Water	100	2.0	92	<sup>60</sup>
4	SMI/ZnCl <sub>2</sub>	DMF	–	20 (min)	94	<sup>63</sup>
5	Zinc(II) L-prolinate	Water	100	2.0	91	<sup>61</sup>
6	UiO-66/Sal-ZnCl <sub>2</sub>	Water	60	2.0	98	This study

**Table 3.** Comparison of UiO-66/Sal-ZnCl<sub>2</sub> catalyst with other catalysts that used for the synthesis of 1-benzyl-4-phenyl-1 H-1,2,3-triazole.

### Data availability

The data sets used and analyzed during the current study are available in supplementary information.

Received: 6 July 2024; Accepted: 11 October 2024

Published online: 20 October 2024

### References

- Hu, Z. et al. Metal–Organic frameworks-based frustrated Lewis pairs for selective reduction of nitroolefins to Nitroalkanes. *J. Am. Chem. Soc.* **146**, 17924–17930 (2024).
- Karmakar, A. et al. Guedes, Thiophene-Functionalized Cadmium (II)-Based Metal–Organic Frameworks for CO<sub>2</sub> Adsorption with Gate-Opening Effect, Separation, and Catalytic Conversion. *Inorg. Chem.* **63**, 13321–13337 (2024).
- Nikseresh, A., Ghoochi, F. & Mohammadi, M. Postsynthetic modification of Amine-Functionalized MIL-101 (cr) metal–Organic frameworks with an EDTA–Zn (II) complex as an effective Heterogeneous Catalyst for Hantzsch synthesis of Polyhydroquinolines. *ACS Omega.* **9**, 28114–28128 (2024).
- Ghobakhloo, F., Mohammadi, M., Ghaemi, M. & Azarifar, D. Post-synthetic generation of amino-acid-functionalized UiO-66-NH<sub>2</sub> metal–Organic Framework nanostructures as an Amphoteric Catalyst for Organic reactions. *ACS Appl. Nano Mater.* **7**, 1265–1277 (2024).
- Farrusseng, D., Aguado, S. & Pinel, C. Metal–organic frameworks: Opportunities for catalysis. *Angew Chem. Int. Ed.* **48**, 7502–7513 (2009).
- Chughtai, A. H., Ahmad, N., Younus, H. A., Laypkov, A. & Verpoort, F. Metal–organic frameworks: Versatile heterogeneous catalysts for efficient catalytic organic transformations. *Chem. Soc. Rev.* **44**, 6804–6849 (2015).
- Huang, Y. B., Liang, J., Wang, X. S. & Cao, R. Multifunctional metal–organic framework catalysts: Synergistic catalysis and tandem reactions. *Chem. Soc. Rev.* **46**, 126–157 (2017).
- Li, X. et al. Preparation of promising anode materials with Sn-MOF as precursors for superior lithium and sodium storage. *J. Alloys Compd.* **842**, 155605 (2020).
- Dong, H. et al. Regulation of metal ions in smart metal-cluster nodes of metal-organic frameworks with open metal sites for improved photocatalytic CO<sub>2</sub> reduction reaction. *Appl. Catal. B Environ.* **276**, 119173 (2020).
- Jiao, S. et al. The synthesis of an antifungal 1,2,4-triazole drug and the establishment of a drug delivery system based on zeolitic imidazolate frameworks. *New. J. Chem.* **43**, 18823–18831 (2019).

11. Tan, Q. et al. A temperature-responsive smart molecular gate in a metal-organic framework for task-specific gas separation. *J. Mater. Chem.* **7**, 26574–26579 (2019).
12. Zhao, J., Wang, C., Wang, S. & Zhou, Y. Experimental and DFT study of selective adsorption mechanisms of pb(II) by UiO-66-NH<sub>2</sub> modified with 1,8- dihydroxyanthraquinone. *J. Ind. Eng. Chem.* **83**, 111–122 (2020).
13. Wang, A. et al. Robust Ru/Ce@Co Catalyst with an optimized support structure for Propane Oxidation. *Environ. Sci. Technol.* **58**, 12742–12753 (2024).
14. Ghobakhloo, F., Azarifar, D., Mohammadi, M., Keypour, H. & Zeynali, H. Copper (II) Schiff-base complex modified UiO-66-NH<sub>2</sub> (Zr) metal-organic framework catalysts for Knoevenagel condensation–Michael addition–cyclization reactions. *Inorg. Chem.* **61**, 4825–4841 (2022).
15. Giri, P. K., Parihar, V., Kumar, S. & Nagaraja, C. M. Copper nanoparticles anchored on the metal–Organic Framework as Recyclable Catalyst for CO<sub>2</sub> fixation to high-value compounds. *ACS Appl. Nano Mater.* **7**, 15488–15497 (2024).
16. Dhakshinamoorthy, A. & Garcia, H. Catalysis by metal nanoparticles embedded on metal-organic frameworks. *Chem. Soc. Rev.* **41**, 5262–5284 (2012).
17. Cohen, S. M. The postsynthetic renaissance in porous solids. *J. Am. Chem. Soc.* **139**, 2855–2863 (2017).
18. Kaur, M. et al. Post-synthesis modification of metal-organic frameworks using Schiff base complexes for various catalytic applications. *J. Chem. Eng.* **423**, 130230 (2021).
19. Deria, P. et al. Beyond post-synthesis modification: Evolution of metal-organic frameworks via building block replacement. *Chem. Soc. Rev.* **43**, 5896–5912 (2014).
20. Bai, Y. et al. Zr-based metal-organic frameworks: Design, synthesis, structure, and applications. *Chem. Soc. Rev.* **45**, 2327–2367 (2016).
21. Cavka, J. H. A new zirconium inorganic building brick forming metal-organic frameworks with exceptional stability. *J. Am. Chem. Soc.* **130**, 13850–13851 (2008).
22. Ahmadijokani, F. et al. UiO-66 metal-organic frameworks in water treatment: A critical review. *Prog Mater. Sci.* **125**, 100904 (2022).
23. Rego, R. M., Kurkuri, M. D. & Kigga, M. A comprehensive review on water remediation using UiO-66 MOFs and their derivatives. *Chemosphere.* **302**, 134845 (2022).
24. Liu, H. et al. Modified UiO-66 as photocatalysts for boosting the carbon-neutral energy cycle and solving environmental remediation issues. *Coord. Chem. Rev.* **458**, 214428 (2022).
25. Pourmadadi, M. et al. UiO-66 metal-organic framework nanoparticles as gifted MOFs to the biomedical application: A comprehensive review. *J. Drug Deliv Sci. tec.* **76**, 103758 (2022).
26. Feng, Y., Chen, Q., Jiang, M. & Yao, J. Tailoring the properties of UiO-66 through defect engineering: A review. *Ind. Eng. Chem. Re.* **58**, 17646–17659 (2019).
27. Liu, X. Metal-organic framework UiO-66 membranes. *Front. Chem. Sci. Eng.* **14**, 216–232 (2020).
28. Motaghi, H., Arabkhani, P., Parvinnia, M. & Asfaram, A. Simultaneous adsorption of cobalt ions, azo dye, and imidacloprid pesticide on the magnetic chitosan/activated carbon@ UiO-66 bio-nanocomposite: Optimization, mechanisms, regeneration, and application. *Sep. Purif. Technol.* **284**, 120258 (2022).
29. Ghasemzadeh, M. A., Mirhosseini-Eshkevari, B., Tavakoli, M. & Zamani, F. Metal-organic frameworks: Advanced tools for multicomponent reactions. *Green. Chem.* **22**, 7265–7300 (2020).
30. Mirhosseini-Eshkevari, B., Esnaashari, M. & Ghasemzadeh, M. A. Novel Brønsted acidic ionic liquids confined in UiO-66 nanocages for the synthesis of dihydropyrido[2,3d]pyrimidine derivatives under solvent-free conditions. *ACS Omega.* **4**, 10548–10557 (2019).
31. Mirhosseini-Eshkevari, B., Ghasemzadeh, M. A. & Esnaashari, M. Highly efficient and green approach for the synthesis of spirooxindole derivatives in the presence of novel Brønsted acidic ionic liquids incorporated in UiO-66 nanocages. *Appl. Organomet. Chem.* **33**, 5027–5040 (2019).
32. Mirhosseini-Eshkevari, B., Ghasemzadeh, M. A., Esnaashari, M. & Ganjali, S. T. Introduction a novel Brønsted acidic ionic liquid incorporated in UiO-66 nanocages for the efficient synthesis of pyrimido[4,5-d]pyrimidines. *Chem. Select.* **4**, 12920–12927 (2019).
33. Azarifar, D., Ghorbani-Vaghei, R., Daliran, S. & Oveisi, A. R. A multifunctional zirconium-based metal-organic framework for the one-pot tandem photooxidative Passerini three-component reaction of alcohols. *ChemCatChem.* **9**, 1992–2000 (2017).
34. Erfaninia, N., Tayebee, R., Dusek, M. & Amini, M. M. Ethylene diamine grafted nanoporous UiO-66 as an efficient basic catalyst in the multi-component synthesis of 2-aminothiophenes. *Appl. Organomet. Chem.* **32**, 4307–4317 (2018).
35. Ghorbani-Vaghei, R., Azarifar, D., Daliran, S. & Oveisi, A. R. The UiO-66-SO<sub>3</sub>H metal-organic framework as a green catalyst for the facile synthesis of dihydro-2-oxypyrrrole derivatives. *RSC Adv.* **6**, 29182–29189 (2016).
36. Shaabani, A., Mohammadian, R., Hooshmand, S. E., Hashemzadeh, A. & Amini, M. M. Zirconium metal-organic framework (UiO-66) as a robust catalyst toward solvent-free synthesis of remarkable heterocyclic rings. *Chem. Select.* **2**, 11906–11911 (2017).
37. Arefi, E., Khojastehnezhad, A. & Shiri, A. A magnetic copper organic framework material as an efficient and recyclable catalyst for the synthesis of 1,2,3-triazole derivatives. *Sci. Rep.* **11**, 20514 (2021).
38. Arefi, E., Khojastehnezhad, A. & Shiri, A. A core-shell superparamagnetic metal-organic framework: A recyclable and green catalyst for the synthesis of propargylamines. *New. J. Chem.* **45**, 21342–21349 (2021).
39. Taghavi, F. et al. Design and synthesis of a new magnetic metal organic framework as a versatile platform for immobilization of acidic catalysts and CO<sub>2</sub> fixation reaction. *New. J. Chem.* **45**, 15405–15414 (2021).
40. Keyhaniyan, M., Shiri, A., Eshghi, H. & Khojastehnezhad, A. Synthesis, characterization and first application of covalently immobilized nickel-porphyrin on graphene oxide for Suzuki cross-coupling reaction. *New. J. Chem.* **42**, 19433–19441 (2018).
41. Ghadamyari, Z., Shiri, A., Khojastehnezhad, A. & Seyedi, S. M. Zirconium (IV) porphyrin graphene oxide: A new and efficient catalyst for the synthesis of 3,4-dihydropyrimidin-2(1H)-ones. *Appl. Organomet. Chem.* **33**, 5091 (2019).
42. Matin, M. M. et al. Triazoles and their derivatives: Chemistry, synthesis, and therapeutic applications. *Front. Mol. Biosci.* **9**, 864286 (2022).
43. Dai, J., Tian, S., Yang, X. & Liu, Z. Synthesis methods of 1,2,3-/1,2,4-triazoles: A review. *Front. Chem.* **10**, 891484 (2022).
44. Jaiswal, S. et al. Emerging approaches for synthesis of 1,2,3-triazole derivatives. A review. *Org. Prep Proc. Inter.* **54**, 387–422 (2022).
45. Yadav, S. et al. Harnessing the untapped catalytic potential of a CoFe<sub>2</sub>O<sub>4</sub>/Mn-BDC hybrid MOF composite for obtaining a multitude of 1,4-disubstituted 1,2,3-triazole scaffolds. *Inorg. Chem.* **59**, 8334–8344 (2020).
46. Jia, X., Xu, G., Du, Z., Fu, Y. & Cu (BTC)-MOF catalyzed multicomponent reaction to construct 1,4-disubstituted-1,2,3-triazoles. *Polyhedron.* **151**, 515–519 (2018).
47. Wang, Z., Zhou, X., Gong, S. & Xie, J. MOF-Derived Cu@ NC catalyst for 1,3-dipolar cycloaddition reaction. *Nanomaterials.* **12**, 1070 (2022).
48. Castillo, J-C. et al. Water-Compatible synthesis of 1,2,3-Triazoles under Ultrasonic conditions by a Cu(I) complex-mediated click reaction. *ACS Omega.* **5**, 30148–30159 (2020).
49. Du, Z., Li, B., Jiang, C., Sun, R. & Chen, S. Sorption of U (VI) on Schiff-base functionalized metal-organic frameworks UiO-66-NH<sub>2</sub>. *J. Radioanal Nucl. Chem.* **327**, 811–819 (2021).
50. Wang, K., Gu, J. & Yin, N. Efficient removal of pb(II) and cd(II) using NH<sub>2</sub>-functionalized Zr-MOFs via rapid microwave-promoted synthesis. *Ind. Eng. Chem. Res.* **56**, 1880–1887 (2017).
51. Tian, F., Weng, R., Huang, X., Chen, G. & Huang, Z. Fabrication of silver-doped UiO-66-NH<sub>2</sub> and characterization of antibacterial materials. *Coatings.* **12**, 1939 (2022).

52. Lili, L., Xin, Z., Jinsen, G. & Chunming, X. Engineering metal-organic frameworks immobilize gold catalysts for highly efficient one-pot synthesis of propargylamines. *Green. Chem.* **14**, 1710–1720 (2012).
53. Leus, K. et al. A Mo-grafted metal organic framework: A synthesis, characterization and catalytic investigations. *J. Catal.* **316**, 201–209 (2014).
54. Song, Q., Jia, M. K., Ma, W. H., Fang, Y. F. & Huang, Y. P. Heterogeneous degradation of toxic organic pollutants by hydrophobic copper Schiff-base complex under visible irradiation. *Sci. China Chem.* **56**, 1775–1782 (2013).
55. Kandiah, M. et al. Synthesis and stability of tagged UiO-66 Zr-MOFs. *Chem. Mater.* **22**, 6632–6640 (2010).
56. Trivedi, M. K., Sethi, K. K., Panda, P. & Jana, S. A comprehensive physicochemical, thermal, and spectroscopic characterization of zinc (II) chloride using X-ray diffraction, particle size distribution, differential scanning calorimetry, thermogravimetric analysis/differential thermogravimetric analysis, ultraviolet-visible, and fourier transform-infrared spectroscopy. *Int. J. Pharm. Investig.* **7**, 33–40 (2017).
57. Veisi, H. et al. Pd immobilization biguanidine modified Zr-UiO-66 MOF as a reusable heterogeneous catalyst in Suzuki–Miyaura coupling. *Sci. Rep.* **11**, 21883 (2021).
58. Hou, J. et al. Synthesis of UiO-66-NH<sub>2</sub> derived heterogeneous copper (II) catalyst and study of its application in the selective aerobic oxidation of alcohols. *J. Mol. Catal. Chem.* **407**, 53–59 (2015).
59. Morozova, M. A. et al. Regioselective Zn(OAc)<sub>2</sub>-catalyzed azide–alkyne cycloaddition in water: the green click-chemistry. *Org. Chem. Front.* **4**, 978–985 (2017).
60. Ghadamyari, Z., Khojastehnezhad, A., Seyedi, S. M., Taghavi, F. & Shiri, A. Graphene oxide functionalized Zn(II) salen complex: An efficient and new route for the synthesis of 1,2,3-triazole derivatives. *Chem. Select.* **5**, 10233–10242 (2020).
61. Kidwai, M. & Jain, A. Regioselective synthesis of 1,4-disubstituted triazoles using bis(L)prolinato-N,O]zn complex as an efficient catalyst in water as a sole solvent. *Appl. Organometal Chem.* **25**, 620–625 (2011).
62. Meng, X., Xu, X., Gao, T. & Chen, B. Zn/C-Catalyzed cycloaddition of Azides and Aryl Alkynes. *Eur. J. Org. Chem.* 5409–5414 (2010).
63. Daraie, M., Heravi, M. & Sarmasti, N. Synthesis of polymer-supported Zn(II) as a novel and green nanocatalyst for promoting click reactions and using design of experiment for optimization of reaction conditions. *J. Macromol. Sci. Chem. A.* **57**, 488–498 (2020).

## Acknowledgements

The authors gratefully acknowledge the Research Council of Ferdowsi University of Mashhad (3/57052).

## Author contributions

MR and AK designed and planned the catalyst, the experiments, and the final analyses. MR contributed with AK to perform the analyses of the results and wrote the initial manuscript with consulting with AS. AS supervised the finding results and provided critical feedback on the final main manuscript. All authors reviewed the manuscript.

## Declarations

### Competing interests

The authors declare no competing interests.

### Additional information

**Supplementary Information** The online version contains supplementary material available at <https://doi.org/10.1038/s41598-024-76199-y>.

**Correspondence** and requests for materials should be addressed to A.S.

**Reprints and permissions information** is available at [www.nature.com/reprints](http://www.nature.com/reprints).

**Publisher's note** Springer Nature remains neutral with regard to jurisdictional claims in published maps and institutional affiliations.

**Open Access** This article is licensed under a Creative Commons Attribution-NonCommercial-NoDerivatives 4.0 International License, which permits any non-commercial use, sharing, distribution and reproduction in any medium or format, as long as you give appropriate credit to the original author(s) and the source, provide a link to the Creative Commons licence, and indicate if you modified the licensed material. You do not have permission under this licence to share adapted material derived from this article or parts of it. The images or other third party material in this article are included in the article's Creative Commons licence, unless indicated otherwise in a credit line to the material. If material is not included in the article's Creative Commons licence and your intended use is not permitted by statutory regulation or exceeds the permitted use, you will need to obtain permission directly from the copyright holder. To view a copy of this licence, visit <http://creativecommons.org/licenses/by-nc-nd/4.0/>.

© The Author(s) 2024